

Electromagnetic Sensing System for Ore Waste Classification and Grade Detection in LHD Buckets

RJ. Exposito Marcano¹

1. Department of Civil, Environmental and Natural Resources Engineering, Luleå University of Technology, Luleå, SE-971 87, Sweden.

Abstract

Underground mines that employ the sublevel caving (SLC) method often suffer from significant levels of ore dilution due to the technique of extracting ore through gravity flow. When the ore is blasted and falls into drifts, it creates drawpoints where Load-Haul-Dump (LHD) vehicles collect the fragmented material and transport it to its destination or a subsequent transportation system. LHDs are equipped with a load cell in the arm, which measures the weight of the material in the bucket. This weight enables distinguishing between waste material and ore, due to the different rock properties, and approximate the ore grade in the bucket. However, this measurement presents challenges when, for example, both rocks have similar density, or when actual bucket load, fragmentation, and water content vary significantly in each loading. This inability to discern accurately leads to increases in operational cost, inefficiencies in transportation, and energy waste. The study focuses on the Kiirunavaara mine case and investigates the feasibility of an electromagnetic sensing system concept for the LHD bucket, capable of distinguishing between magnetite-rich iron ore and waste based on their intrinsic electromagnetic properties. This work focuses on modeling a sensing system using the AC/DC module of COMSOL Multiphysics® software. The problem setup includes a 2D model of an LHD bucket partially filled and a sensor array composed of excitation and detection coils placed along the outer bucket walls. A primary magnetic field and a resulting induced field are monitored to evaluate differences in magnetic flux density and eddy current distribution, to distinguish ore from waste, and to approximate ore grade. Simulations suggest that the sensor system is susceptible to the spatial arrangement of ore versus waste inside the bucket. Specifically, the presence of high-permeability zones (iron ore) results in significant contrasts in magnetic field intensity and distribution patterns. In addition, results support the feasibility of the technique to monitor ore grade in LHD's bucket immediately after loading and laying the groundwork for a future prototype validation. If successful, this system could contribute to smarter underground operations, real-time material classification, and reduced dilution.

Keywords: Electromagnetic sensing, iron ore mining, ore classification, Load-Haul-Dump (LHD) systems.

Introduction

In SLC mines, the blasted ore flows by gravity into the production drifts. Extracting material generates voids that induce detachment of the surrounding rock mass, allowing rock from above to flow in and fill the muck pile at the drawpoint [1], [2]. This caving phenomenon can also detach gangue, causing a mix between ore and waste material, increasing the amount of material expected to be extracted, and causing dilution, which is one major disadvantage of the SLC method [3]. Dilution increases costs, which can make the drawpoint uneconomical, leading to abandoning the front and proceeding to another [4]. Monitoring is crucial to quantify waste inflow and estimate ore grade variations to maximize ore recovery and to properly decide when to stop loading from certain drawpoints [5]. Ore grade variations can be detected through visual differentiation of ore and waste based on color, shape, and texture; manual systematic sampling and assay of the muck piles; and weighing the material on the LHD bucket if the density between ore and waste significantly differs [6].

Visual differentiation is not always possible since it depends on how different ore and waste are and on the capability of the operator or system to

differentiate them, which increases the margin of error [6]. Sampling the muck piles can provide a highly accurate value of ore grade; however it demands manpower and requires stopping the operations in the drawpoint to take the samples, which are time-consuming and high-cost factors [5], [6].

In the case of the Kiirunavaara mine, density-based monitoring is employed due to the substantial difference between waste (2,700 kg/m³) and iron ore (4,600 kg/m³) specific weight. The ore is loaded from drawing points by Load Haul Dump (LHD) machines, which are equipped with a load cell that weighs the ore in the bucket to subsequently estimate the ore percentage in the bucket, providing a continuous measurement of ore grade [6].

This estimation is given by empirical formulas, which assume a constant swell factor, specific bucket fill, and a linear relationship between bucket weight and ore grade [7]. However, these parameters do not behave in such a way, which discredits the accuracy of the estimate. The assumptions are invalid due to the following reasons [7]:

- Ore fragmentation varies, causing voids of different dimensions between the rock fragments. Therefore, the same apparent volume will have different weights depending on how

large the interstices are, resulting in the assignment of different ore grades.

- LHDs do not load the exact same volume every time. Bucket volumes can differ from their theoretical capacity. Measurements of higher or lower weights may not correlate with the assumed volume.
- Moisture content is not considered, which can significantly affect the ore grade measurements when, for example, the amount of water is considerably high, which causes incorrect higher-grade estimations.

Therefore, including a monitoring system that can provide ore grade measurements to corroborate the values from the density-based estimation can enhance the ore recovery.

In the case of the Kiirunavaara mine, the orebody's economic mineral is magnetite (Fe_3O_4). The iron ore consists of fine-grained magnetite-apatite with an average grade of 63.8% Fe, and in some instances, it can reach approximately ~70% Fe, with fractions exceeding 90% magnetite [8]. Since the ore content is dominated by magnetite, it inherits intrinsic magnetic properties that can be exploited to distinguish ore from waste, i.e., monitoring can be achieved without relying on the specific weight but using other properties instead.

Most minerals are diamagnetic or paramagnetic, and few of them exhibit ferromagnetism, with the magnetite being the most common one and the most important when determining the magnetic permeability of a rock [9].

This study uses a simple conceptual design to investigate the influence of different rock grain sizes and distribution-based variation of relative magnetic permeability in a domain. The model presented is a preliminary monitoring concept to estimate grade and discriminate iron ore and waste from relative magnetic permeability (μ_r) instead of specific weight.

Theory

Minerals exhibit ferromagnetism when large groups of atoms orient themselves together toward a field due to intense polarization [9]. These orientation changes of magnetic domains enhance significantly the magnetic field strength (H). As field strength increases, the magnetic domains align with the external magnetic field, which enhances magnetic induction (B).

The electromagnetic induction in rocks depends on the relationship between the rock mass and the governing equation

$$B = \mu H \quad (1)$$

Where μ is the magnetic permeability of the medium. In most cases, the magnetic permeability of a rock is determined by its magnetite content (Figure 1), since unlike other iron minerals such as ilmenite, pyrrhotite, hematite, or pyrite, which have permeabilities >2.5 , magnetite can present values ranging from 2.5 to 16 [9].

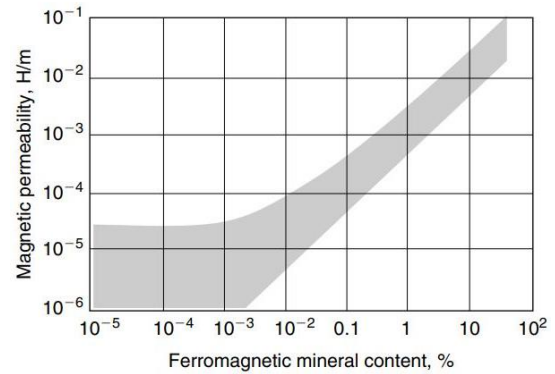


Figure 1. Magnetic permeability as a function of ferromagnetic mineral fractions in intrusive igneous rocks [9].

The permeability of ferromagnetic materials varies because the rearrangement of magnetic domains is limited by the material's crystal structure, reaching its maximum when the domains are aligned with the magnetic field as much as the crystal structure permits [10]. At this point, the magnetization of the material no longer increases, which means that the incremental permeability approaches the permeability of the free space ($\mu_0 \approx 4\pi \times 10^{-7} H/m$). Therefore, further increases of the magnetic field strength H will hardly increase the magnetic induction B , and the material is said to have reached its saturation state [10].

In the case of magnetite-rich iron ore, this exhibits a high low-field (incremental) permeability μ_r , so small increases in H produce large increases in B . Then, as the magnetite fraction decreases, a much smaller increase in B will occur for the same H . Thus, measuring the low-field slope or the approach to saturation are robust indicators for differentiating magnetite-rich ore, mixed ore, and waste rock (Figure 2).

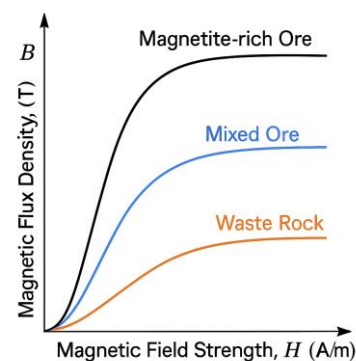


Fig 2. Representative $B-H$ curves of expected response of magnetite-rich ore, mixed ore, and waste rock.

Numerical Model

The conceptual monitoring system model is analyzed using the COMSOL® AC/DC Module, specifically through the Magnetic Fields (mf) and Electrical Circuit (cir) interfaces. A time-dependent study was conducted to solve the magnetic field and induced current distributions, which allows for the

subsequent computation of the incremental mutual inductance (M) between the driving coil and the passive coils in a determined time window (t_1, t_2). The concept is simulated in a magneto-quasi static regime ($v = 0$), so the motional term in total current density ($\sigma v \times B$) vanishes. At the beginning of each simulation run, the initial conditions ($t = 0$) are set to zero, and boundary conditions impose $n \cdot B = 0$ by applying magnetic insulation ($n \times A = 0$) on the outer air domain. Table 1 summarizes the governing equations in the model.

Table 1: Governing equations and constitutive relations of the model

Description	Equation
Ampère's law	$\nabla \times H = J$ (2)
Magnetic flux density	$B = \nabla \times A$ (3)
Electric field	$E = -\frac{\partial A}{\partial t} - \nabla V$ (4)
Total current density	$J = \sigma E + J_e$ (5)
Linear isotropic constitutive law	$B = \mu_0 \mu_r(x, y) H$ (6)
Current density (drive coil)	$J_e = \frac{N I_{drive}(t)}{A} e_{coil}$ (7)
Induced current density (sense coils)	$J_e = \frac{N I_{sense}(t)}{A} e_{coil}$ (8)

The model consists of 22 domains of five different types of entities: an E-shaped core, coils, a high-strength steel plate (LHD bucket), ore, and air (Figure 3).

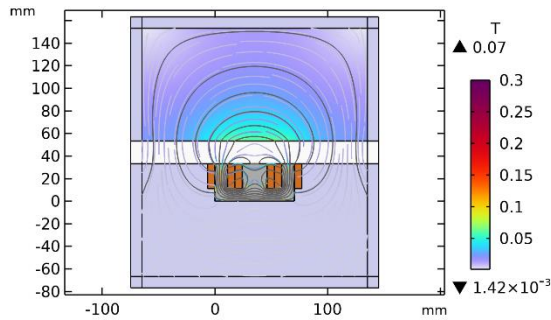


Figure 3. 2D model of the coil-ore-coil setup.

The middle coil is a driving coil, which has a current ramp as

$$I_{drive}(t) = kt \quad (9)$$

Where k is a constant integer is used to increase the current in relation to time. The incremental current I_{drive} induces a current I_{sense} in the adjacent passive coils according to Faraday's law of induction. Thus, the influence of the relative permeability $\mu_r(x, y)$ of the ore over the magnetic flux is observed when computing the I_{sense} distribution.

The coils are homogenized multiturn conductors. The sense coils are connected to an external circuit with a resistor $R_{sense} = 1\Omega$, and are solved via

$$V = R_{sense} I_{sense} \quad (10)$$

After a brief $\frac{L_{sense}}{R_{sense}}$ transient the I_{sense} distribution becomes constant and obeys

$$L_{sense} \frac{dI_{sense}}{dt} + R I_{sense} = M \frac{dI_{drive}}{dt} = Mk \quad (11)$$

$$I_{sense} = \frac{M}{R_{sense}} k \quad (12)$$

L_{sense} , denotes the self-inductance of the sense coil short-circuited through R_{sense} .

The distribution of the incremental mutual inductance (M) is calculated by averaging I_{sense} over the time window $[t_1 = 3s, t_2 = 5s]$ as follows

$$M = \frac{R}{k} \overline{I_{sense}}_{[t_1, t_2]} \quad (13)$$

Several distributions of M for different average values of ore relative magnetic permeability $\mu_r(x, y)$, by using parametric sweep in time-dependent study. M distribution provides a single robust comparable value across the runs, independent of the ramp slope k and the resistor R in the sense coils.

Ore domain and Mesh

The ore relative magnetic permeability $\mu_r(x, y)$ is either a homogenous constant (ideal case) or a heterogeneous random field (rock mass). This emulates the variability of iron ore along plane XY due to different grain sizes, different iron minerals, and normal deviations of magnetite permeability values.

The ore domain is split into tiles of predefined size (L_g), which are assigned a pseudorandom permeability value (Figures 4 & 5).

The ore domain partition is achieved by

$$i = \left\lfloor \frac{x - x_0}{L_g} \right\rfloor; \quad j = \left\lfloor \frac{y - y_0}{L_g} \right\rfloor \quad (14)$$

Then, an analytic function u computes a pseudo-random number per tile using a hash of the indices (a, b, & c) and a *seed*, which changes the spatial arrangement while keeping the same statistics.

$$u = \text{mod}(\sin(ai + bj + \text{seed})c, 1) \quad (15)$$

The average value of the analytic function u_{Avg} is subtracted from each u , and subsequently used with a predefined coefficient of variation (cv) to obtain the distribution function of relative magnetic permeability:

$$u_0 = u - u_{Avg} \quad (16)$$

$$f(x, y) = 1 + cv u_0 \quad (17)$$

$$\mu_r^{raw}(x, y) = \mu_{mean} f(x, y) \quad (18)$$

$$\mu_r(x, y) = \max(\mu_{min}, \min(\mu_{max}, \mu_r^{raw})) \quad (19)$$

Examples of the resulting permeability distribution given by function $\mu_r(x, y)$ across the ore domain are illustrated in Figures 4 and 5.

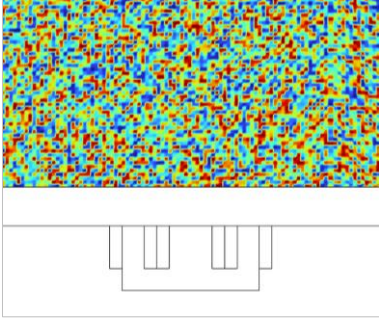


Figure 4. Example 1 of a heterogeneous relative magnetic permeability field $\mu_r(x, y)$ for $L_g = 2[\text{mm}]$.

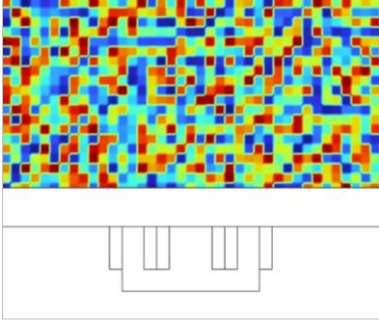


Figure 5. Example 2 of a heterogeneous relative magnetic permeability field $\mu_r(x, y)$ for $L_g = 5[\text{mm}]$.

The parameter cv controls the amplitude of deviations around μ_{mean} , such that if $cv = 0$, then the ore domain is homogeneous ($f(x, y) = 0$). Similarly, if $cv > 0$, then the tile's permeability deviates from the mean (e.g., $0.2 = 20\%$).

The final relative magnetic permeability function is obtained by scaling the fluctuation of $\mu_r^{raw}(x, y)$ to the target μ_{mean} , and clamping the final field to μ_{min} and μ_{max} , which are the physical limits of the magnetite (~ 2.5 to 16) [9].

Once the physical limits are established, the distribution of the permeability in the ore domain is changed by modifying the values of L_g , cv , and $seed$, such that different cases can be studied. Table 2 presents the specific levels used in the parametric sweep.

Table 2: Parameter sweep settings for L_g , cv , and μ_{mean}

Parameter	Level
$L_g[\text{mm}]$	1, 2, 5, 10, 20
cv	0, 0.5, 1, 2, 5
$\mu_{mean}[\text{H/m}]$	2, 4, 6, 8, 10, 12, 14, 16

The minimum tile size was set to $L_g = 1\text{mm}$, since below this threshold no noticeable differences were observed, so it prevents unnecessary mesh refinement and reduces computational time (Figure 6). Also, bounds on L_g and cv were chosen based on literature descriptions of Kiirunavaara iron ore [8].

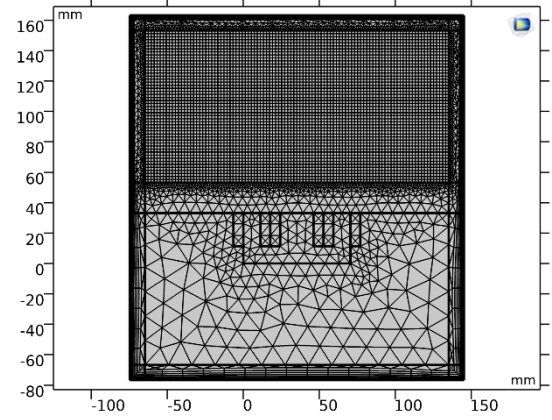


Figure 6. User-controlled mesh of conceptual monitoring system, with refined elements ($L_g = 2\text{mm}$) along the ore domain.

Simulation Results

In this section induced current in the sense coil (I_{sense}) and the mutual inductance (M) distributions are presented for both homogeneous and heterogeneous ore domains, considering different values of mean magnetic relative permeability.

Homogeneous ore domain

The induced current in the sense coils for the homogeneous ore domain (Figure 7) exhibits a rapid increase, followed by a flat plateau within 0.5s , showing a transient response. I_{sense} reaches a steady state for $t > 0.5\text{s}$, corresponding to the maximum I_{sense} for determined μ_{mean} . Maximum I_{sense} attainable increases with the μ_{mean} of the ore domain. Moreover, the incremental gain diminishes as μ_{mean} increases, so the maximum I_{sense} values become closer together.

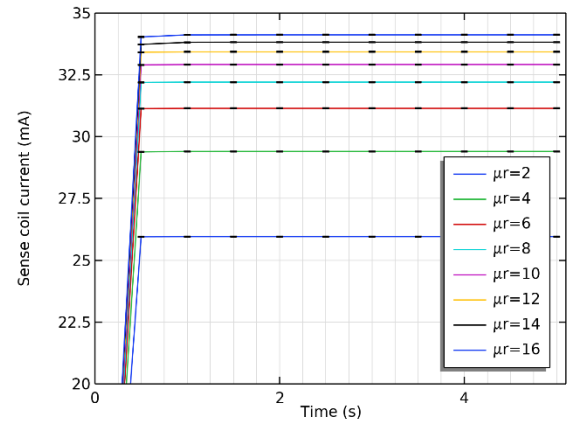


Figure 7. Sense coil current versus time for constant relative magnetic permeability along homogeneous ore domain.

The steady state provides a stable window $[t_1, t_2]$ to compute the mutual inductance (M). M is computed for the time window from $t_1 = 3\text{s}$ to $t_2 = 5\text{s}$. The relationship between M and μ_{mean} (Figure 8) shows concave-down trend, where the incremental gain decreases for higher μ_{mean} , reaching a total variation of $\sim 30\%$ difference from the minimum to maximum

limit permeabilities (range for magnetite) for the studied geometry. This behavior of the M curve, similar to the B-H curve, establishes a direct indicator for estimating ore grade and differentiating ore from waste.

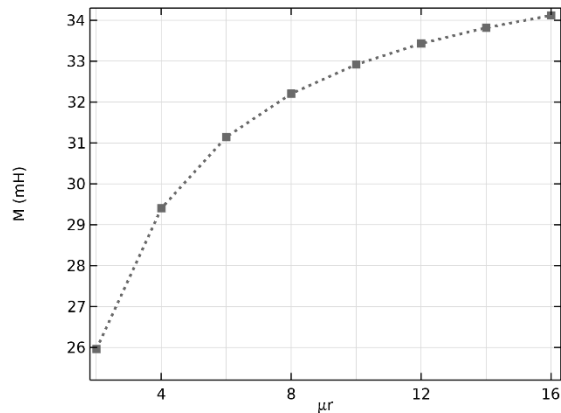


Figure 8. Mutual inductance versus relative magnetic permeability for homogeneous ore domain.

Heterogeneous ore domain

Heterogeneity was introduced by varying the spatial distribution of relative magnetic permeability with $\mu_r(x, y)$. This is restricted to a minimum, a maximum, and an average value of relative permeability of the ore domain.

Figure 9 presents the relation between cv and M . As cv increases, the ore domain displays stronger spatial fluctuations in relative permeability between tiles. The plot shows that high heterogeneity (larger cv) leads to lower mutual inductance M , which differs significantly from the homogeneous case. An example is when the rock texture exhibits magnetite crystals scattered among other non-magnetic minerals. However, for reduced mean relative permeabilities ($\mu_{mean} < 4 H/m$), this difference is significantly lower than for high mean relative permeabilities, suggesting that the mutual magnetization would carry a lower error when used for ore-waste differentiation than for ore grade estimation in highly heterogeneous rocks.

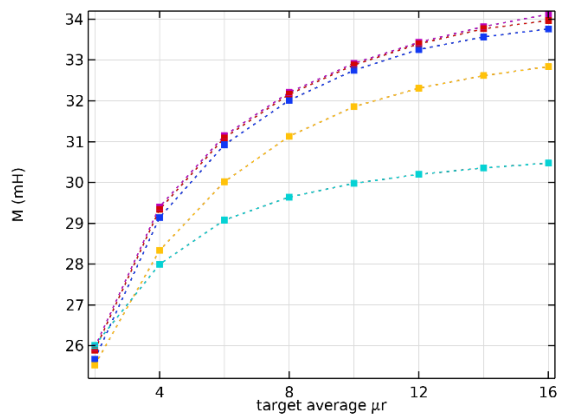


Figure 9. Mutual inductance versus relative magnetic permeability for different levels of cv across heterogeneous ore domain.

On the other hand, the influence of different sizes of rock crystals is simulated by the different levels of L_g (Figure 10).

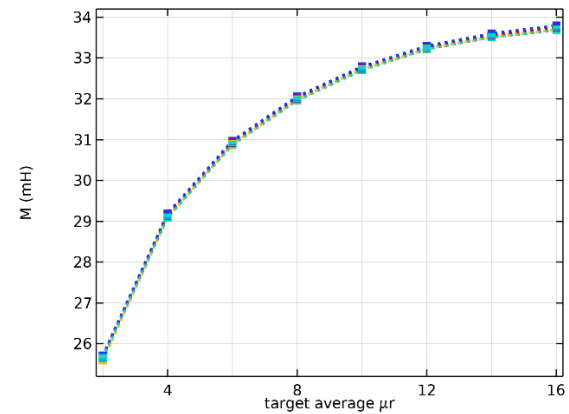


Figure 10. Mutual inductance versus relative magnetic permeability for different levels of L_g across heterogeneous ore domain.

No significant changes in M occurred for $L_g < 20mm$ across the different tested levels of μ_{mean} . Therefore, in fine-grained rocks, deviations of M are expected only when flux crosses substantially large non-magnetic inclusions.

Concluding remarks

This study explored a magnetic-based monitoring concept as an alternative to density-based monitoring systems for improving ore-grade estimation during loading of magnetite-rich iron ore. The current LHD's density-based ore grade monitoring system used in the Kiirunavaara mine presents challenges due to the rock fragmentation, loading volume variation, and moisture content. These issues increase the difficulty of monitoring continuously and precisely during loading.

The magnetic-based monitoring concept presented shows promising result for both ore-waste differentiation and grade estimation, demonstrating sensitivity to variations in magnetic permeability within the range of magnetite.

The results indicate that mutual inductance can serve as a single, robust metric for tracking the ore's effective low-field permeability and consequently its grade. The concept operates with DC in the magneto-quasi-static regime, such that at the used ramp rates, conductivity (linked to moisture) is expected to have negligible influence, and the response is primarily dominated by permeability contrasts. However, future studies should evaluate the influence of water content, natural joints, and common mineral structures such as rock veins on the mutual inductance response.

As the results are geometry-specific and assume linear incremental B-H behavior, experimental future work should include the obtention of non-linear B-H curves for the different specific types of iron ore present in the Kiirunavaara mine and validation against drill-core grades data.

Finally, comparing simulations across different fragment positions and fragmentation levels with field measurements would allow the obtention of calibration coefficients to improve future ore-grade estimations.

References

- [1] D. H. Laubscher, “Cave mining—the state of the art,” *Journal of The Southern African Institute of Mining and Metallurgy*, vol. 94, no. 10, pp. 279–293, 1994.
- [2] E. W. Cokayne, “Sublevel caving Chapter 1: Introduction,” *Underground mining methods handbook*, pp. 872–879, 1982.
- [3] R. Kvapil, “Gravity flow of granular materials in Hoppers and bins in mines—II. Coarse material,” in *International journal of rock mechanics and mining sciences & geomechanics abstracts*, 1965, pp. 277–292.
- [4] D. Nilsson, “Planning economics of sublevel caving,” *Underground mining methods handbook. New York: Society of Mining Engineers of the American Institute of Mining, Metallurgical and Petroleum Engineers, Inc*, pp. 953–960, 1982.
- [5] C. R. Quinteiro, L. Larsson, and W. A. Hustrulid, “Theory and practice of very-large-scale sublevel caving,” *Underground mining methods: engineering fundamentals and international case studies*, vol. 8307, pp. 381–384, 2001.
- [6] G. Shekhar, A. Gustafson, A. Hersinger, K. Jonsson, and H. Schunnesson, “Development of a model for economic control of loading in sublevel caving mines,” *Mining Technology*, vol. 128, no. 2, pp. 118–128, Apr. 2019, doi: 10.1080/25726668.2019.1586371.
- [7] S. Manzoor, A. Gustafson, and H. Schunnesson, “Challenges with Density-Based Grade Estimation at LKAB’s Underground Iron Ore Mines,” *Min Metall Explor*, vol. 39, no. 6, pp. 2301–2310, Dec. 2022, doi: 10.1007/s42461-022-00688-9.
- [8] K. P. Niiranen, “Characterization of the Kiirunavaara iron ore deposit for mineral processing with a focus on the high silica ore type B2,” 2015.
- [9] M. S. Zhdanov, “Electromagnetic properties of rocks and minerals,” 2009, pp. 395–447. doi: 10.1016/S0076-6895(08)00210-2.
- [10] W. M. Telford, L. P. Geldart, and R. E. Sheriff, *Applied geophysics*. Cambridge university press, 1990.

Acknowledgements

This work was supported by the Wallenberg Foundation’s Jubilee Grant.